# Semianalytic Stress-Function Variational Approach for the Interfacial Stresses in Bonded Joints

Xiang-Fa Wu, M.ASCE[1]; and Robert A. Jenson[2]

**Abstract:** High interfacial stresses near the edges of bonded joints are responsible for their debonding failure. This paper reports a new semianalytic stress-function variational approach to the interfacial stresses of a bonded joint, which is made of a straight tension bar covered with a reinforcing patch and subjected to mechanical loads and/or uniform change of temperature. The process introduces two interfacial shear and normal stress functions, which are correlated via the approximately same radius of curvature of the slender adherends. All the stress components in the joint are expressed in terms of the interfacial stress functions based on the classic Euler-Bernoulli beam theory and equilibrium equations of elasticity. Deformation compatibility of the joint is satisfied by minimizing the complementary strain energy, which leads to a fourth-order ordinary differential equation (ODE) of the interfacial shear stress function. The interfacial shear and normal stresses are determined explicitly and compared with those given by the elementary beam theory and FEM, respectively. The results gained in this study are applicable to scaling analysis of joint strength and optimization of structural design of joints. The present formalism can be extended conveniently to the mechanical stress and thermal stress analysis of various bonded structures, including adhesively bonded joints, composite joints, and recently developed flexible electronics. **DOI: 10.1061/(ASCE)EM.1943-7889.0000803.** © *2014 American Society of Civil Engineers.*

**Author keywords:** Interfacial stress; Free-edge stress; Thermal stress; Bonded joints; Energy method; Elasticity.



## Introduction

Bonded joints are fundamental structural components that have found broad application in load transfer and connection of separated parts. Bonded joints typically consist of two adherends of the same or dissimilar materials joined together via bolts, solders, or adhesives. In engineering practice, soldered joints are extensively used in ground vehicles and marine ships, whereas adhesively bonded joints (ABJs) find application in aerospace structures, especially those made of fiber-reinforced polymer matrix composites (PMCs) (Jones 1999). For bonded joints (e.g., lap, strap, and butt joints) subjected to external loading and/or change of environmental temperature, high interfacial stresses are typically triggered near the free edges because of a mismatch of Poisson's ratios and coefficients of thermal expansion of the adherends. These interfacial stresses are responsible for the debonding failure of bonded joints. Without a doubt, understanding of the stress state near the free edges of bonded joints can provide information particularly useful in joint design, structural optimization, and failure analysis. Yet, accurate stress analysis of bonded joints has long been a challenging task because of the constraints of multiple boundary conditions (BCs) and dissimilar materials, in particular when combined with rate effects and material nonlinearity. As a matter of fact, strength and failure analysis of multimaterial joints is still a priority research field in aerospace materials and structures as addressed in the annual board agency announcement (BAA) of the U.S. Air Force Office of Scientific Research (AFOSR).

The concept of free-edge stress was conceived by Timoshenko (1925), who first considered the deflection of bimetal thermostats subjected to uniform change of temperature. Goland and Reissner (1944) were the first to systematically investigate the interfacial stresses in a single-lap joint subjected to axial tension, in which the adherends were in the state of combined in-plane tension and deflection. An approximate solution was gained for this practical elasticity problem; however, except for a few specified locations, this approach did not satisfy all the traction BCs. Meanwhile, with the fast development of microelectronics since the 1970s, thermal stress-induced debonding failure in electronics packaging has become one of the main technical concerns and has attracted exceptional research in the last three decades. Among others, Chen and Nelson (1979) and Suhir (1986, 1989) proposed two simplified engineering solutions to the edge stress of bimaterials (chips). Suhir's solution (1986) did not satisfy the fundamental static equilibrium equations of the joint and free traction BCs because of the oversimplified formulation and introduction of multiple ad hoc assumptions (including several coarse revisions made later). Theoretically, because of the existence of stress singularity near the sharp free edges, detailed finite-element analysis (FEA) shows that the edge stresses are expected to grow rapidly with refining of the mesh size at the free edges. More recently, with the birth of flexible electronics based on smart deposition of rigid microsilicon units onto compliant polymeric substrates (Khang et al. 2006; Sun et al. 2006; Kim and Rogers 2008), significant efforts have been dedicated to understanding their mechanical response and durability that highly depend upon the interfacial stress between the free-standing silicon islands and the flexible substrate layers (Jiang et al. 2007, 2008; Lu et al. 2007; Yoon et al. 2007; Song et al. 2008; Khang et al. 2009). It is expected that consistent, accurate prediction of these interfacial stresses would benefit the structural design for sound mechanical durability of these novel intelligent flexible electronics (e.g., flexible displayers, intelligent rubber surgical gloves) (Gates 2009).

[1]Assistant Professor, Dept. of Mechanical Engineering, North Dakota State Univ., Fargo, ND 58108-6050 (corresponding author). E-mail: xiangfa.wu@ndsu.edu

[2]Graduate Student, Dept. of Mechanical Engineering, North Dakota State Univ., Fargo, ND 58108-6050.

Note. This manuscript was submitted on June 13, 2013; approved on April 2, 2014; published online on April 30, 2014. Discussion period open until September 30, 2014; separate discussions must be submitted for individual papers. This paper is part of the ***Journal of Engineering Mechanics***, © ASCE, ISSN 0733-9399/04014089(11)/$25.00.

On the other hand, stress analysis of bonded joints has been an active topic of research in structural engineering and materials science for decades owing to its technical importance to structural durability and strength analysis. Recent representative studies include those by Yuan et al. (2004) and De Lorenzis and Teng (2007) for the full-range mechanical behavior of joints made of fiber-reinforced PMCs and concrete, Carpinteri et al. (2009) for the debonding failure analysis of ABJs in RC, and Yang et al. (2004) and Yang and Guan (2009) for the nonlinear response of adhesive single-lap composite joints and stress distribution in adhesive tubular torsion joints. A detailed review of the historical development and recent progress of stress analysis of bonded joints was made recently by da Silva et al. (2009a, b). Yet, when dealing with the adhesive layer, investigations reported in the literature typically adopted the assumption of a shear-lag model, which considers the adhesive layers as two independent elastic springs in axial and lateral directions, respectively. Examination of the shear-lag model shows that this model does not satisfy the generalized Hooke's law, nor do the interfacial shear stresses obtained from the model satisfy the stress-free condition at the joint edges. Thus, refined work in improving the stress analysis of bonded joints and guaranteeing the extendibility of the techniques of stress analysis for broad applications is still desired.

Furthermore, compared with stress analysis of bonded joints, remarkable progress has been made in parallel studies of cracking in bonded layers since the 1990s. Quite a few crack models have been proposed to extract the fracture characteristics [e.g., stress intensity factor (SIF) and crack tip opening displacement (CTOD)] of cracked layers (Suo and Hutchinson 1990; Hutchinson and Suo 1992; Li 2001; Yu and Hutchinson 2001, 2003; Wu and Dzenis 2002a, b; Wu et al. 2003a, b, 2004, 2008). In addition, a significant number of classic SIF solutions of cracked layers have been well documented in two classic SIF handbooks by Sih (1973) and Tada et al. (1973). It is obvious that improved stress analysis of bonded joints can facilitate the fracture analysis of bonded joints and therefore lead to in-depth understanding of failure mechanisms and damage evolution in bonded joints.

Since the 1990s, several improved methods for stress analysis of bonded joints have been reported in the literature. For instance, by expressing the interfacial shear and normal stresses in terms of Fourier series with the coefficients determined by minimizing the complementary strain energy of the joint, Chang (1990, 1993) obtained the explicit expressions of joint stresses that can satisfy all the traction BCs. Yin (1994a, b) and Wu and Dzenis (2005) determined the free-edge stresses of laminated composites by using a stress-function variational method. In this approach, interface stress functions were directly introduced, through which all the stress equilibrium equations and stress continuity across the laminate interfaces were satisfied intrinsically; deformation compatibility was fulfilled via minimization of the complementary strain energy of the laminate that led to a set of ordinary differential equations (ODE) solved by eigenfunctions. All the free-edge traction BCs in this approach can be completely satisfied. Compared with the free-edge stresses of laminates predicted by detailed FEA, the stress-function variational method can predict the accurate stress variation at interfaces of laminates with a distance of approximately one ply thickness out of the free edges (Wu 2009).

Along this avenue, this work introduces a new semianalytic stress-function variational approach to the interfacial stresses of bonded joints by directly adopting two interfacial shear and normal stress functions. With these two stress functions, all the stress components in the joints are approximated within the framework of classic Euler-Bernoulli beam theory (for axial stress) and two-dimensional (2D) elasticity (for shear and transverse normal stress), which can satisfy all the stress equilibrium equations and traction BCs of the joints. The governing equation of the stress functions is obtained via minimization of the complementary strain energy of the joints. As a result, all the stress components can be determined in explicit expressions. Comparisons of the current results with those based on the elementary beam theory, FEM, and those available in the literature will be made. Potential applications of the current study will be further addressed.

## Problem Formulation and Solution

Consider a bonded joint consisting of a straight tension bar (substrate) and a reinforcing patch, as illustrated in Fig. 1. Both the tension bar and reinforcing patch are considered prismatic segments such that the reinforcing patch has the length $L$, thickness $h_1$, and width $b$, and the tension bar has the thickness $h_2$, width $b$, and length much larger than $L$. The coordinate systems are introduced as follows. The $x$-coordinate is selected from the symmetric midplane to direct the bar axis, and $y_1$ and $y_2$ are the vertical coordinates with the origins located at the centroids of cross sections of the reinforcing patch and tension bar, respectively. The joint is subjected to uniform tension $p_0$ far away from the reinforcing patch and uniform change of temperature $\Delta T$ relative to the reference temperature of stress-free state. Because of the mismatch of material properties across the interface, high interfacial shear and normal (peeling) stresses are triggered near the patch ends, as Fig. 1(b) illustrates. These interfacial stresses are responsible for the failure of bonded joints, such as interface debonding commonly observed in engineered joints. Rigidly speaking, the patch ends are in a complicated three-dimensional (3D) stress state due to the effect of dissimilar Poisson's ratios of the adherends. To simplify the process, hereafter the authors treat the joint in the state of either plane-stress or plane-strain. Before applying the mechanical loads or uniform temperature change, no residual stress is assumed in the joint at the reference temperature. In addition, the tension bar and reinforcing patch are dealt with as isotropic, linearly thermoelastic solids. For the convenience of the upcoming derivations, parameters and variables with subscripts 1 and 2 are attached to the reinforcing patch (cover) and the tension bar (substrate), respectively.

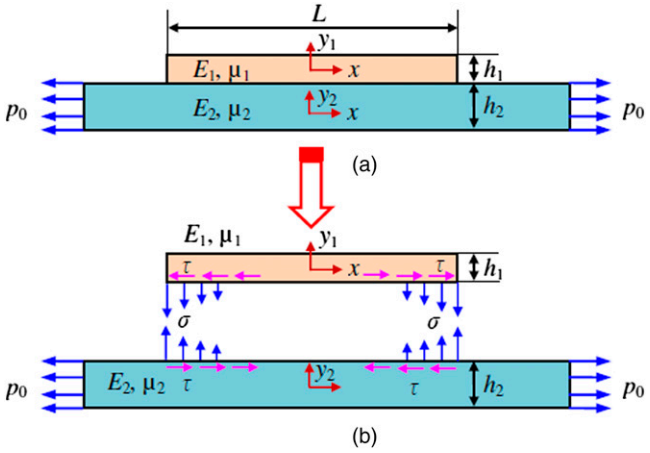


**Fig. 1.** Schematic of bonded joint: (a) bonded joint consists of a tension bar covered with a reinforcing patch; (b) schematic interfacial shear and normal stresses

### Static Equilibrium Equations and Deformation Compatibility

Owing to loss of lateral symmetry, deformation of the joint is a combination of in-plane elongation and lateral deflection. The reinforcing patch and tension bar are considered to be slender and therefore can be approached as Euler-Bernoulli beams. Fig. 2 shows free-body diagrams (FBDs) of the typical segmental elements of the reinforcing patch and tension bar, in which the stress components and stress resultants are defined to follow the standard sign conventions (Beer et al. 2009). Given a representative segmental element of the reinforcing patch [Fig. 2(a)], the corresponding equilibrium equations are

$$\Sigma F_x = 0: \frac{dS_1}{dx} = -b\tau \tag{1}$$

$$\Sigma F_y = 0: \frac{dQ_1}{dx} = -b\sigma \tag{2}$$

$$\Sigma M = 0: \frac{dM_1}{dx} = Q_1 - \frac{h_1}{2}(b\tau) \tag{3}$$

Similarly, for a representative segmental element of the tension bar [Fig. 2(b)], the relevant equilibrium equations are

$$\Sigma F_x = 0: \frac{dS_2}{dx} = b\tau \tag{4}$$

$$\Sigma F_y = 0: \frac{dQ_2}{dx} = b\sigma \tag{5}$$

$$\Sigma M = 0: \frac{dM_2}{dx} = Q_2 - \frac{h_2}{2}(b\tau) \tag{6}$$

To simplify the process, the authors use an approximate deformation-compatibility such that the slender reinforcing patch and the tension bar have the same radius of curvature

$$\frac{M_1}{E_1 I_1} = \frac{M_2}{E_2 I_2} \tag{7}$$

where

$$I_1 = \frac{1}{12} b h_1^3 \quad \text{and} \quad I_2 = \frac{1}{12} b h_2^3 \tag{8}$$

Eq. (7) is used to correlate the interfacial shear and normal stresses along the bonding line in the upcoming derivation, which significantly simplifies the governing equation of the problem.

### Stress Resultants

Define the interfacial shear stress $\tau$ and normal stress $\sigma$ as two unknown functions to be determined:

$$\tau = f(x) \quad \text{and} \quad \sigma = g(x) \tag{9}$$

Symmetry of the bonded joint with respect to the midspan ($y$-axis) requires that $f(x)$ be an odd function and $g(x)$ be an even function, i.e.

$$f(-x) = -f(x) \quad \text{and} \quad g(-x) = g(x) \tag{10}$$

At the patch ends, shear-free condition reads

$$f(-L/2) = f(L/2) = 0 \tag{11}$$

Stress resultants of the adherends can be expressed in terms of $f$ and $g$ as follows. Integration of Eq. (1) with respect to $x$ from $x = -L/2$ yields

$$\int_{-L/2}^{x} dS_1 = -\int_{-L/2}^{x} bf(\xi)d\xi \tag{12}$$

With the aid of the traction-free condition at $x = -L/2$, i.e., $S_1(-L/2) = 0$, the normal stress resultant (axis force) Eq. (12) can be expressed as

$$S_1(x) = -b\int_{-L/2}^{x} f(\xi)d\xi \tag{13}$$

Integration of Eq. (2) with respect to $x$ from $x = -L/2$ leads to

$$\int_{-L/2}^{x} dQ_1 = -\int_{-L/2}^{x} bg(\xi)d\xi \tag{14}$$

With the shear-free condition at $x = -L/2$, i.e., $Q_1(-L/2) = 0$, the shear stress resultant (shear force) Eq. (14) can be rewritten as

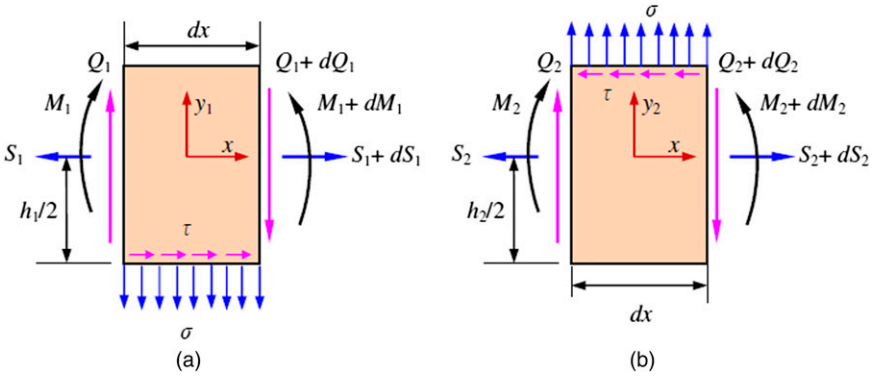


**Fig. 2.** Free-body diagrams of representative segmental element of (a) slender reinforcing patch; (b) slender tension bar

$$Q_1(x) = -b \int_{-L/2}^{x} g(\xi)d\xi \tag{15}$$

Furthermore, integration of Eq. (3) with respect to $x$ from $x = -L/2$ gives

$$\int_{-L/2}^{x} dM_1 = \int_{-L/2}^{x} \left[Q_1(\xi) - \frac{h_1}{2}(b\tau)\right]d\xi \tag{16}$$

By triggering the moment-free condition at $x = -L/2$, i.e., $M_1(-L/2) = 0$, the bending moment Eq. (16) becomes

$$M_1(x) = -b \int_{-L/2}^{x} \int_{-L/2}^{\xi} g(\varsigma)d\varsigma d\xi - \frac{bh_1}{2} \int_{-L/2}^{x} f(\xi)d\xi \tag{17}$$

By using the same procedure, integration of Eq. (4) with respect to $x$ from $x = -L/2$ yields

$$\int_{-L/2}^{x} dS_2 = \int_{-L/2}^{x} bf(\xi)d\xi \tag{18}$$

With the axial traction condition at $x = -L/2$, i.e., $S_2(-L/2) = p_0 bh_2$, the normal stress resultant (axis force) Eq. (18) can be expressed as

$$S_2(x) = p_0(bh_2) + b \int_{-L/2}^{x} f(\xi)d\xi \tag{19}$$

The shear force $Q_2(x)$ and bending moment $M_2(x)$ can be determined correspondingly by integrating Eqs. (5) and (6) with respect to $x$ from $x = -L/2$ and using the stress-free conditions at $x = -L/2$

$$Q_2(x) = b \int_{-L/2}^{x} g(\xi)d\xi \tag{20}$$

$$M_2(x) = b \int_{-L/2}^{x} \int_{-L/2}^{\xi} g(\varsigma)d\varsigma d\xi - \frac{bh_2}{2} \int_{-L/2}^{x} f(\xi)d\xi \tag{21}$$

In addition, $f$ and $g$ can be correlated through the deformation compatibility [Eq. (7)]

$$\frac{E_2 I_2}{E_1 I_1}\left[-\int_{-L/2}^{x} \int_{-L/2}^{\xi} g(\varsigma)d\varsigma d\xi - \frac{h_1}{2} \int_{-L/2}^{x} f(\xi)d\xi\right] = \int_{-L/2}^{x} \int_{-L/2}^{\xi} g(\varsigma)d\varsigma d\xi - \frac{h_2}{2} \int_{-L/2}^{x} f(\xi)d\xi \tag{22}$$

Differentiating at both sides of Eq. (22) yields

$$f(x) = -2\frac{\eta_0}{h_2} \int_{-L/2}^{x} g(\xi)d\xi, \tag{23}$$

where $\eta_0 = (e_{21}h_{21}^3 + 1)/(e_{21}h_{21}^2 - 1)$; $e_{21} = E_2/E_1$; and $h_{21} = h_2/h_1$. As a result, the bending moments $M_1(x)$ and $M_2(x)$ in Eqs. (17) and (21) can be rewritten as

$$M_1(x) = -\frac{bh_1}{2}\left(1 - \eta_0^{-1}h_{21}\right) \int_{-L/2}^{x} f(\xi)d\xi \tag{24}$$

$$M_2(x) = -\frac{bh_2}{2}\left(1 + \eta_0^{-1}\right) \int_{-L/2}^{x} f(\xi)d\xi \tag{25}$$

One special case needs to be mentioned: When the joint satisfies the condition $e_{21}h_{21}^2 = 1$, it leads to $f(x) = 0$ and Eq. (23) does not hold. In the following derivation, the discussion of this trivial case is ignored.

## Stress Components

### Stresses in the Reinforcing Patch

For slender adherends of the joint, axial normal stress of the reinforcing patch can be approached according to the flexural stress formula of Euler-Bernoulli beams:

$$\sigma_{xx}^{(1)} = \frac{S_1}{bh_1} - \frac{M_1 y_1}{I_1} = -\left[\frac{1}{h_1} - \frac{6y_1}{h_1^2}\left(1 - \frac{4}{3}\eta_0^{-1}h_{21}\right)\right] \int_{-L/2}^{x} f(\xi)d\xi \tag{26}$$

Shear stress $\tau_{y_1x}^{(1)}$ in the reinforcing patch can be determined by integrating the equilibrium equation

$$\frac{\partial \sigma_{xx}}{\partial x} + \frac{\partial \tau_{y_1x}^{(1)}}{\partial y_1} = 0 \tag{27}$$

with respect to $y_1$ from an arbitrary location $y$ to the top surface at $y_1 = h_1/2$

$$\int_{y_1}^{h_1/2} \frac{\partial \sigma_{xx}^{(1)}}{\partial x} dy_1 + \int_{y_1}^{h_1/2} \frac{\partial \tau_{y_1x}^{(1)}}{\partial y_1} dy_1 = 0 \tag{28}$$

which leads to

$$\tau_{y_1x}^{(1)} = -\left[\frac{1}{h_1}\left(\frac{h_1}{2} - y_1\right) - \frac{3}{h_1^2}\left(\frac{h_1^2}{4} - y_1^2\right)\left(1 - \frac{4}{3}\eta_0^{-1}h_{21}\right)\right] f(x) \tag{29}$$

Here, the traction-free condition $\tau_{y_1x}^{(1)}(h_1/2) = 0$ has been implemented. Furthermore, normal stress $\sigma_{y_1y_1}^{(1)}$ in the patch layer can be calculated by integrating the equilibrium equation

$$\frac{\partial \sigma^{(1)}_{y_1y_1}}{\partial y_1} + \frac{\partial \tau^{(1)}_{xy_1}}{\partial x} = 0 \tag{30}$$

with respect to $y_1$ from an arbitrary location $y$ to the top surface at $y_1 = h_1/2$ as

$$\int_{y_1}^{h_1/2} \frac{\partial \sigma^{(1)}_{y_1y_1}}{\partial y_1} dy_1 + \int_{y_1}^{h_1/2} \frac{\partial \tau^{(1)}_{xy_1}}{\partial x} dy_1 = 0 \tag{31}$$

which yields

$$\sigma^{(1)}_{y_1y_1} = -\left\{ \frac{1}{h_1}\left[\frac{h_1}{2}\left(\frac{h_1}{2} - y_1\right) - \frac{1}{2}\left(\frac{h_1^2}{4} - y_1^2\right)\right] - \frac{3}{h_1^2}\left[\frac{h_1^2}{4}\left(\frac{h_1}{2} - y_1\right) - \frac{1}{3}\left(\frac{h_1^3}{8} - y_1^3\right)\right]\left(1 - \frac{4}{3}\eta_0^{-1}h_{21}\right)\right\} f'(x) \tag{32}$$

**Stresses in the Substrate Bar**

Stress components in the tension bar can be determined using the same approach. The axial normal stress can be approximated as

$$\sigma^{(2)}_{xx} = \frac{S_2}{bh_2} - \frac{M_2 y_2}{I_2} = p_0 + \left[\frac{1}{h_2} + \frac{6y_2}{h_2^2}\left(1 + \frac{4}{3}\eta_0^{-1}\right)\right] \int_{-L/2}^{x} f(\xi) d\xi \tag{33}$$

Shear stress $\tau^{(2)}_{y_2x}$ can be obtained by integrating the equilibrium equation

$$\frac{\partial \sigma^{(2)}_{xx}}{\partial x} + \frac{\partial \tau^{(2)}_{y_2x}}{\partial y_2} = 0 \tag{34}$$

with respect to $y_2$ from the bottom surface $y_2 = h_2/2$ to an arbitrary location $y_2$ of the tension bar

$$\int_{-h_2/2}^{y_2} \frac{\partial \sigma^{(2)}_{xx}}{\partial x} dy_2 + \int_{-h_2/2}^{y_2} \frac{\partial \tau^{(2)}_{y_2x}}{\partial y_2} dy_2 = 0 \tag{35}$$

which leads to

$$\tau^{(2)}_{y_2x} = -\left[\frac{1}{h_2}\left(y_2 + \frac{h_2}{2}\right) + \frac{3}{h_2^2}\left(y_2^2 - \frac{h_2^2}{4}\right)\left(1 + \frac{4}{3}\eta_0^{-1}\right)\right] f(x) \tag{36}$$

Here, the stress-free condition $\tau^{(2)}_{y_2x}(-h_2/2) = 0$ has been used. Furthermore, normal stress $\sigma^{(2)}_{y_2y_2}$ in the tension bar can be determined by integrating the equilibrium equation

$$\frac{\partial \sigma^{(2)}_{y_2y_2}}{\partial y_2} + \frac{\partial \tau^{(2)}_{xy_2}}{\partial x} = 0 \tag{37}$$

with respect to $y_2$ from the bottom surface at $y_2 = -h_2/2$ to an arbitrary location $y_2$ such that

$$\int_{-h_2/2}^{y_2} \frac{\partial \sigma^{(2)}_{y_2y_2}}{\partial y_2} dy_2 + \int_{-h_2/2}^{y_2} \frac{\partial \tau^{(2)}_{xy_2}}{\partial x} dy_2 = 0 \tag{38}$$

which yields

$$\sigma^{(2)}_{y_2y_2} = \left\{ \frac{1}{h_2}\left[\frac{1}{2}\left(y_2^2 - \frac{h_2^2}{4}\right) + \frac{h_2}{2}\left(y_2 + \frac{h_2}{2}\right)\right] + \frac{3}{h_2^2}\left[\frac{1}{3}\left(y_2^3 + \frac{h_2^3}{8}\right) - \frac{h_2^2}{4}\left(y_2 + \frac{h_2}{2}\right)\right]\left(1 + \frac{4}{3}\eta_0^{-1}\right)\right\} f'(x) \tag{39}$$

where the traction-free condition $\sigma^{(2)}_{y_2y_2}(-h_2/2) = 0$ has been adopted.

### Governing Equation of Interfacial Stress Functions

For linearly thermoelastic solids, the strain energy of the entire joint ($|x| \le L/2$) can be expressed as (Timoshenko and Goodier 1951; Chang 1990, 1993; Chen and Cheng 1992; Wu et al. 2008)

$$U = b \int_{-L/2}^{L/2} \int_{-h_1/2}^{h_1/2} \left\{ \frac{1}{2}\left[\sigma^{(1)}_{xx}\varepsilon^{(1)}_{xx} + \sigma^{(1)}_{yy}\varepsilon^{(1)}_{yy}\right] + \frac{1+\upsilon_1}{E_1}\left(\tau^{(1)}_{xy_1}\right)^2 \right\} dx dy_1 + b \int_{-L/2}^{L/2} \int_{-h_2/2}^{h_2/2} \left\{ \frac{1}{2}\left[\sigma^{(2)}_{xx}\varepsilon^{(2)}_{xx} + \sigma^{(2)}_{yy}\varepsilon^{(2)}_{yy}\right] + \frac{1+\upsilon_2}{E_2}\left(\tau^{(2)}_{xy_2}\right)^2 \right\} dx dy_2 \tag{40}$$

Here, $\varepsilon^{(i)}_{xx}$ $(i = 1, 2)$ and $\varepsilon^{(i)}_{yy}$ $(i = 1, 2)$ are the normal strains defined by the generalized Hooke's law of linearly thermoelastic solids. In the plane-stress state, it reads

$$\varepsilon^{(i)}_{xx} = \frac{\sigma^{(i)}_{xx}}{E_i} - \upsilon_i \frac{\sigma^{(i)}_{yy}}{E_i} + \alpha_i \Delta T \tag{41}$$

$$\varepsilon^{(i)}_{yy} = \frac{\sigma^{(i)}_{yy}}{E_i} - \upsilon_i \frac{\sigma^{(i)}_{xx}}{E_i} + \alpha_i \Delta T \tag{42}$$

where $\alpha_i$ $(i = 1, 2)$ = coefficients of thermal expansion of the cover and substrate layers, respectively. In the case of plane-strain state, the corresponding expressions can be obtained by replacing the Young's moduli $E_i$ by $E_i/(1-\upsilon_i^2)$, Poisson's ratios $\upsilon_i$ by $\upsilon_i/(1-\upsilon_i)$, and coefficients of thermal expansion $\alpha_i$ by $(1+\upsilon_i)\alpha_i$, where $i = 1, 2$. The strain energy expressed in Eq. (40) is a functional with respect to the unknown function $f$. According to the theorem of minimum complementary strain energy, the complementary strain energy of the joint reaches a stationary point at static equilibrium, which corresponds to the necessary condition in term of variation of the strain energy equal to zero (Chen and Cheng 1992; Wu et al. 2008):

$$\delta U = 0 \tag{43}$$

or

$$b\int_{-L/2}^{L/2}\int_{-h_1/2}^{h_1/2}\left\{\frac{1}{E_1}\left[\sigma_{xx}^{(1)}\delta\varepsilon_{xx}^{(1)}+\delta\sigma_{xx}^{(1)}\varepsilon_{xx}^{(1)}+\sigma_{y_1y_1}^{(1)}\delta\varepsilon_{y_1y_1}^{(1)}+\delta\sigma_{y_1y_1}^{(1)}\varepsilon_{y_1y_1}^{(1)}\right]+\frac{2(1+\upsilon_1)}{E_1}\tau_{xy_1}^{(1)}\delta\tau_{xy_1}^{(1)}\right\}dxdy_1$$
$$+b\int_{-L/2}^{L/2}\int_{-h_2/2}^{h_2/2}\left\{\frac{1}{E_2}\left[\sigma_{xx}^{(2)}\delta\varepsilon_{xx}^{(2)}+\delta\sigma_{xx}^{(2)}\varepsilon_{xx}^{(2)}+\sigma_{y_1y_1}^{(2)}\delta\varepsilon_{y_1y_1}^{(2)}+\delta\sigma_{y_1y_1}^{(2)}\varepsilon_{y_1y_1}^{(2)}\right]+\frac{2(1+\upsilon_2)}{E_2}\tau_{xy_2}^{(2)}\delta\tau_{xy_2}^{(2)}\right\}dxdy_2=0 \tag{44}$$

where $\delta$ = varational operator with respect to the interfacial shear-stress function $f$. By substituting Eqs. (26), (29), (32), (33), (36), and (39) into Eq. (44) and performing several variational operations and simplifications, the shear-stress function $f$ in plane-strain state satisfies a fourth-order ODE of constant coefficients:

$$F^{(IV)}(\xi)-2pF''(\xi)+q^2F(\xi)+\left[-e_{21}^{-1}+\frac{1}{2}(\alpha_1-\alpha_2)\Delta TE_1\Big/p_0\right]\Big/A_{11}=0 \tag{45}$$

where

$$F(\xi)=F(x/h_1)=-\left(\frac{1}{p_0h_1}\right)\int_{-L/2}^{x}f(x)dx \tag{46}$$

$$p=-A_{12}/(2A_{11}) \tag{47}$$

$$q=\sqrt{A_{22}/A_{11}} \tag{48}$$

$$A_{11}=\left(\frac{1}{20}-\frac{2}{15}\beta_1+\frac{13}{140}\beta_1^2\right)+e_{21}^{-1}h_{21}^3\left(\frac{1}{20}-\frac{2}{15}\beta_2+\frac{13}{140}\beta_2^2\right) \tag{49}$$

$$A_{12}=\left(-\frac{2}{3}+\beta_1-\frac{3}{5}\beta_1^2-\upsilon_1+\beta_1\upsilon_1\right)+e_{21}^{-1}h_{21}\left(-\frac{2}{3}+\beta_2-\frac{3}{5}\beta_2^2-\upsilon_2+\beta_2\upsilon_2\right) \tag{50}$$

$$A_{22}=\left(1+3\beta_1^2\right)+e_{21}^{-1}h_{21}^{-1}\left(1+3\beta_2^2\right) \tag{51}$$

$$\beta_1=1-\eta_0^{-1}h_{21} \tag{52}$$

$$\beta_2=1+\eta_0^{-1} \tag{53}$$

In addition, symmetry of the bonded joint with respect to the $y$-axis requires that $f$ is an odd function and $F(\xi)$ is an even function. In the case of $q>p$, the solution to Eq. (45) has the form

$$F(\xi)=C_1\cosh(\beta\xi)\cos(\gamma\xi)+C_2\sinh(\beta\xi)\sin(\gamma\xi)+\left[e_{21}^{-1}-\frac{1}{2}(\alpha_1-\alpha_2)\Delta TE_1/p_0\right]\Big/\left(q^2A_{11}\right) \tag{54}$$

where $\beta=\sqrt{(p+q)/2}$; $\gamma=\sqrt{(q-p)/2}$; and $C_1$ and $C_2$ are two unknown constants to be determined. Thus, stress function $f$ can be determined as

$$f(x)=-p_0h_1\frac{dF(\xi)}{dx}=-p_0[(C_1\beta+C_2\gamma)\sinh(\beta x/h_1)\cos(\gamma/h_1)+(-C_1\gamma+C_2\beta)\cosh(\beta x/h_1)\sin(\gamma x/h_1)] \tag{55}$$

With the shear-free condition at $x=\pm L/2$, $C_1$ and $C_2$ can be correlated as

$$\kappa=\frac{C_1}{C_2}=\frac{\gamma\sinh[\beta L/(2h_1)]\cos[\gamma L/(2h_1)]+\beta\cosh[\beta L/(2h_1)]\sin[\gamma L/(2h_1)]}{\gamma\cosh[\beta L/(2h_1)]\sin[\gamma L/(2h_1)]-\beta\sinh[\beta L/(2h_1)]\cos[\gamma L/(2h_1)]} \tag{56}$$

As a result, $f$ and $F$ can expressed as

$$f(x)=-C_2p_0[(\kappa\beta+\gamma)\sinh(\beta x/h_1)\cos(\gamma x/h_1)+(-\kappa\gamma+\beta)\cosh(\beta x/h_1)\sin(\gamma x/h_1)] \tag{57}$$

and

$$F(x)=C_2[\kappa\cosh(\beta x/h_1)\cos(\gamma x/h_1)+\sinh(\beta x/h_1)\sin(\gamma x/h_1)]+\left[e_{21}^{-1}-\frac{1}{2}(\alpha_1-\alpha_2)\Delta TE_1/p_0\right]\Big/\left(q^2A_{11}\right) \tag{58}$$

Constant $C_2$ can be determined by the conditions of free axial traction and bending moment at $x=\pm L/2$

$$C_2=\frac{\left[-e_{21}^{-1}+\frac{1}{2}(\alpha_1-\alpha_2)\Delta TE_1/p_0\right]\Big/\left(q^2A_{11}\right)}{\kappa\cosh[\beta L/(2h_1)]\cos[\gamma L/(2h_1)]+\sinh[\beta L/(2h_1)]\sin[\gamma L/(2h_1)]} \tag{59}$$

Moreover, in the case of $p > q$, the solution to Eq. (45) has the form

$$F(\xi) = C_1 \cosh(\beta\xi) + C_2 \cosh(\gamma\xi) + \left[e_{21}^{-1} - \frac{1}{2}(\alpha_1 - \alpha_2)\Delta T E_1/p_0\right] \Big/ (q^2 A_{11}) \tag{60}$$

where $\beta = \sqrt{p + \sqrt{p^2 - q^2}}$; $\gamma = \sqrt{p - \sqrt{p^2 - q^2}}$; and $C_1$ and $C_2$ are again two unknown coefficients to be determined. In this case, $f$ can be expressed as

$$f(x) = -p_0 h_1 \frac{dF}{dx} = -p_0[C_1\beta \sinh(\beta x/h_1) + C_2\gamma \sinh(\gamma x/h_1)] \tag{61}$$

By considering the shear-free and traction-free conditions at $x = \pm L/2$, $C_1$ and $C_2$ can be determined and $f$ can be expressed as

$$f(x) = -C_2 p_0[\kappa\beta \sinh(\beta x/h_1) + \gamma \sinh(\gamma x/h_1)] \tag{62}$$

where

$$\kappa = \frac{C_1}{C_2} = -\frac{\gamma \sinh[\gamma L/(2h_1)]}{\beta \sinh[\beta L/(2h_1)]} \quad \text{and}$$
$$C_2 = \frac{\left[-e_{21}^{-1} + \frac{1}{2}(\alpha_1 - \alpha_2)\Delta T E_1/p_0\right] \Big/ (q^2 A_{11})}{\kappa \cosh[\beta L/(2h_1)] + \cosh[\gamma L/(2h_1)]} \tag{63}$$

Consequently, the stress function $g(x)$ can be determined by Eq. (23) as

$$g(x) = -\frac{h_2}{2\eta_0} f'(x) \tag{64}$$

## Examples and Discussions

### Interfacial Stresses in a Bonded Joint due to Mechanical Loads

In the "Problem Formulation and Solution" section, interfacial shear and normal stresses of a bonded joint are determined explicitly using Eqs. (57), (62), and (64). To validate the presented solutions, the authors first examine the shear force transferred by the interface of the left-half portion of the reinforcing patch. This shear force should be equal to the axial force of the reinforcing patch at the midspan $y = 0$ according to static equilibrium and Eq. (13)

$$S_{10} = -b \int_{-L/2}^{0} f(x)dx \tag{65}$$

In addition, for a slender joint, the axial force $S_{10}$ at the midspan ($y = 0$) of the cover should be approximately equal to that given by the elementary beam theory as follows. Consider the half-joint and corresponding FBDs shown in Fig. 3. By using the transformed section technique of composite beams (Beer et al. 2009), if letting the reinforcing patch be the reference material, the location of the joint centroid $C_0$ in the cross section [see Fig. 3(a)] is

$$\bar{y} = \frac{h_1(h_1/2 + h_2) + e_{21}h_2^2/2}{h_1 + e_{21}h_2} \tag{66}$$

The effective area moment of inertia of the transformed cross section is

$$I_{\text{effective}} = \frac{bh_1^3}{12} + bh_1(h_1/2 + h_2 - \bar{y})^2 + \frac{e_{21}bh_2^3}{12} + e_{21}bh_2(h_2/2 - \bar{y})^2 \tag{67}$$

and the effective bending moment acting at the centroid $C_0$ is

$$M_0 = p_0(bh_2)(\bar{y} - h_2/2) \tag{68}$$

Thus, flexural stress in the reinforcing patch can be expressed as

$$\sigma_{xx}^{(1)} = \frac{p_0 h_2}{h_1 + e_{21}h_2} - \frac{M_0 y}{I_{\text{effective}}} \tag{69}$$

Substitution of Eqs. (66)–(68) into Eq. (69) and then integrating with respect to $y$ over the cross section of the cover layer leads to the effective axial force

$$S'_{10} = b\int_{A_i} \sigma_{xx}^{(1)} dy = \frac{p_0 h_1 h_2}{h_1 + e_{21}h_2} - \frac{M_0}{I_{\text{effective}}} \int_{h_2 - \bar{y}}^{h_1 + h_2 - \bar{y}} y dy = p_0 h_2 \left[\frac{h_1}{h_1 + e_{21}h_2} - \frac{h_2(\bar{y} - h_2/2)(2h_1 + h_2 - 2\bar{y})}{2I_{\text{effective}}}\right] \tag{70}$$

To compare Eqs. (65) and (70), the authors consider a bonded joint made of an aluminum tension bar ($E_2 = 70$ GPa, $\upsilon_2 = 0.34$) reinforced with a steel patch ($E_1 = 200$ GPa, $\upsilon_1 = 0.29$). Assume the geometrical ratios of the joint are $h_1/h_2 = 1/4$, $L/h_2 = 20$. From the previous section, the corresponding parameters of interfacial stress functions $f$ and $g$ are $p = 0.430357$; $q = 1.06882$; $\beta = 0.865787$; $\gamma = 0.565005$; and $\kappa = -2.47821$. Eqs. (55) and (64) yield

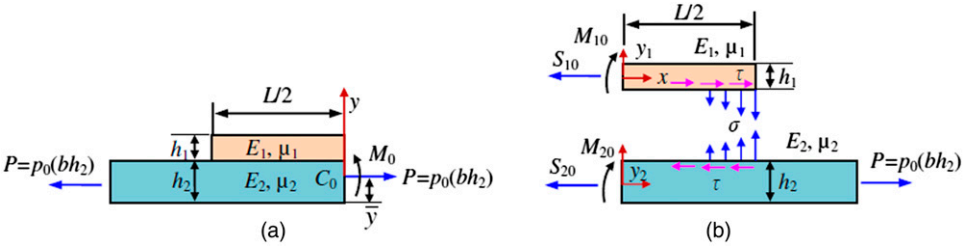


**Fig. 3.** Free-body diagrams of the half-joints for stress resultants at midspan: (a) stress resultants at centroid of cross section; (b) stress resultants of individual adherends at midspan

$$f(x) = 7.24913 \times 10^{-16} p_0 [2.26599 \cosh(0.865787x)\sin(0.565005x) - 1.58059 \sinh(0.865787x)\cos(0.565005x)] \quad (71)$$

$$g(x) = -7.12512 \times 10^{-17} p_0 [-0.0881639 \cosh(0.865787)\cos(0.565005x) + 2.85491 \sinh(0.865787x)\sin(0.565005x)] \quad (72)$$

Substitution of Eq. (71) into Eq. (65) gives the transferred shear force by the reinforcing patch as

$$S_{10} = 0.580789(p_0 h_1) \quad (73)$$

whereas the transformed section technique [Eq. (70)] predicts the axial force at the midspan of the reinforcing patch is

$$S'_{10} = 0.580789(p_0 h_1) \quad (74)$$

The results here indicate an exact convergence of the axial tensile force achieved by the present method at the midspan of a relatively long patch layer using an approach different from the classic beam theory.

In addition, the authors use Eqs. (57), (62), (65), and (70) to further examine the effect of length ratio on the transferred axial force based on the presented approach. Table 1 lists the relative deviations of axial force at the midspan of the reinforcing patch at several length ratios. In the calculation, except for the change of patch length, other parameters are selected from the steel-aluminum joint. Table 1 shows that for short reinforcing patches, a relatively large deviation exists because the classic beam theory does not work well, whereas for a long reinforcing patch, the current method can cover the classic beam theory in calculating the axial force very well. This also validates the accuracy of the present method in the limiting case.

Moreover, to validate the analytic solutions presented earlier, the authors examine the interfacial shear and normal stresses of the steel-aluminum joint subjected to uniform tension in the case of plane-stress state based on the present method and commercial FEM code (*ANSYS 12.0.1*), respectively. The joint being treated is made of a slender aluminum substrate layer ($E_2 = 70$ GPa, $\upsilon_2 = 0.34$) reinforced with a steel patch ($E_1 = 200$ GPa, $\upsilon_1 = 0.29$). The adherends carry the same width, and other geometries are: $h_1 = 2$ mm (steel); $h_2 = 4$ mm (aluminum); and $L = 40$ mm (see Fig. 1). The uniform axial tensile stress of the substrate is assumed to be $p_0 = 1$ MPa. In the linear stress analysis of the joint using *ANSYS*, four-node elements (PLANE182) and mapped uniform quadrilateral meshes are used. Owing to the existence of stress singularity near the free edges, four FEM mesh sizes (i.e., $0.4 \times 0.4$ mm, $0.2 \times 0.2$ mm, $0.1 \times 0.1$ mm, and $0.05 \times 0.05$ mm) are used sequentially to capture the characteristics of the varying free-edge stresses with respect to the mesh size. Figs. 4(a and b) plot variations of the interfacial shear and normal stresses with the distance from the right edge, and Figs. 4(c and d) plot the stress variations in the zoomed range close to the adherend end. The stress comparison shows that the present model can reasonably predict the stress variations along the interface, although the stress values are lower near the adherend end than those predicted by refined FEM results because of the use of lower-order approach.

**Table 1.** Comparison of Relative Deviation of the Midspan Axial Forces in the Reinforcing Patch Based on the Present Method and Classic Transformed Section Technique

| Length ratio ($L/h_2$) | Relative deviation (%) |
|---|---|
| 2 | 3.57 |
| 3 | 1.47 |
| 4 | 0.332 |
| 5 | $3.49 \times 10^{-3}$ |
| 10 | $7.02 \times 10^{-6}$ |

Owing to the existence of stress singularity near the free edge, interfacial stresses predicted by FEM increase rapidly with decreasing mesh size at the free edges. Similar to other analytic models in the literature, the present model cannot predict such stress singularity. However, the good fitting to the interfacial stress variation trends predicted by FEM indicates the validity of the present method that can be used for scaling analysis, design, and optimization of joint structures, etc.

### Interfacial Stresses in a Bimaterial Thermostat due to Thermal Loads

Thermal stress analysis of a bonded joint, as shown in Fig. 1, induced by pure temperature change is equivalent to that of a bimaterial thermostat. In the following, we consider the thermal stresses in an aluminum/molybdenum thermostat as studied by Suhir (1986, 1989), Eischen et al. (1990) and Ru (2002). In terms of the symbol system used in this work, the system parameters are $E_1 = 70$ GPa; $\upsilon_1 = 0.345$; $\alpha_1 = 23.6 \times 10^{-6}/°\text{C}$; $h_1 = 2.5$ mm; $E_2 = 325$ GPa; $\upsilon_2 = 0.293$; $\alpha_2 = 4.9 \times 10^{-6}/°\text{C}$; $h_2 = 2.5$ mm; $L = 50.8$ mm; and $\Delta T = 240°\text{C}$. Plane-strain state is assumed in the present simulation. The resulting interfacial shear stress $\tau$ and normal stress $\sigma$ can be expressed explicitly by Eqs. (62) and (64):

$$\tau = 6.60932 \times 10^{-9} \left[2.33459 \sinh(0.933937x) - 1.04659 \times 10^{-9} \sinh(1.7813x)\right] (\text{MPa}) \quad (75)$$

$$\sigma = 5.24334 \times 10^{-9} \left[2.18013 \cosh(0.933937x) - 1.86429 \times 10^{-9} \cosh(1.7813x)\right] (\text{MPa}) \quad (76)$$

Figs. 5(a and b) show the distribution of the thermal shear and normal stresses along the interface due to a uniform change of temperature. From the figure, high concentrations of shear and normal stresses can be detected near the free edges, and the stress variations along the interface are close to those given by Eischen et al. (1990) and Ru (2002). Specifically, the peak value of interfacial normal stress $\sigma_{\max} = 103.7$ MPa is close to the one predicted by Eischen et al. (1990) ($\sigma_{\max} = 102.8$ MPa), and $\tau_{\max} = 36.07$ MPa appears at a distance close to $L/25$ from the free edges that is slightly lower than those given in the literature.

In addition, it needs to be mentioned that introduction of the approximate deformation compatibility [Eq. (7)] dramatically simplifies the process and makes it possible to gain the explicit expressions of interfacial stresses along the bonding line. Yet, the accuracy of these interfacial stresses is lower than those obtained by FEM based on fine meshes. Furthermore, Wu and Jenson (2011), Wu and Zhao (2013), and Wu et al. (2014) also performed the study to treat

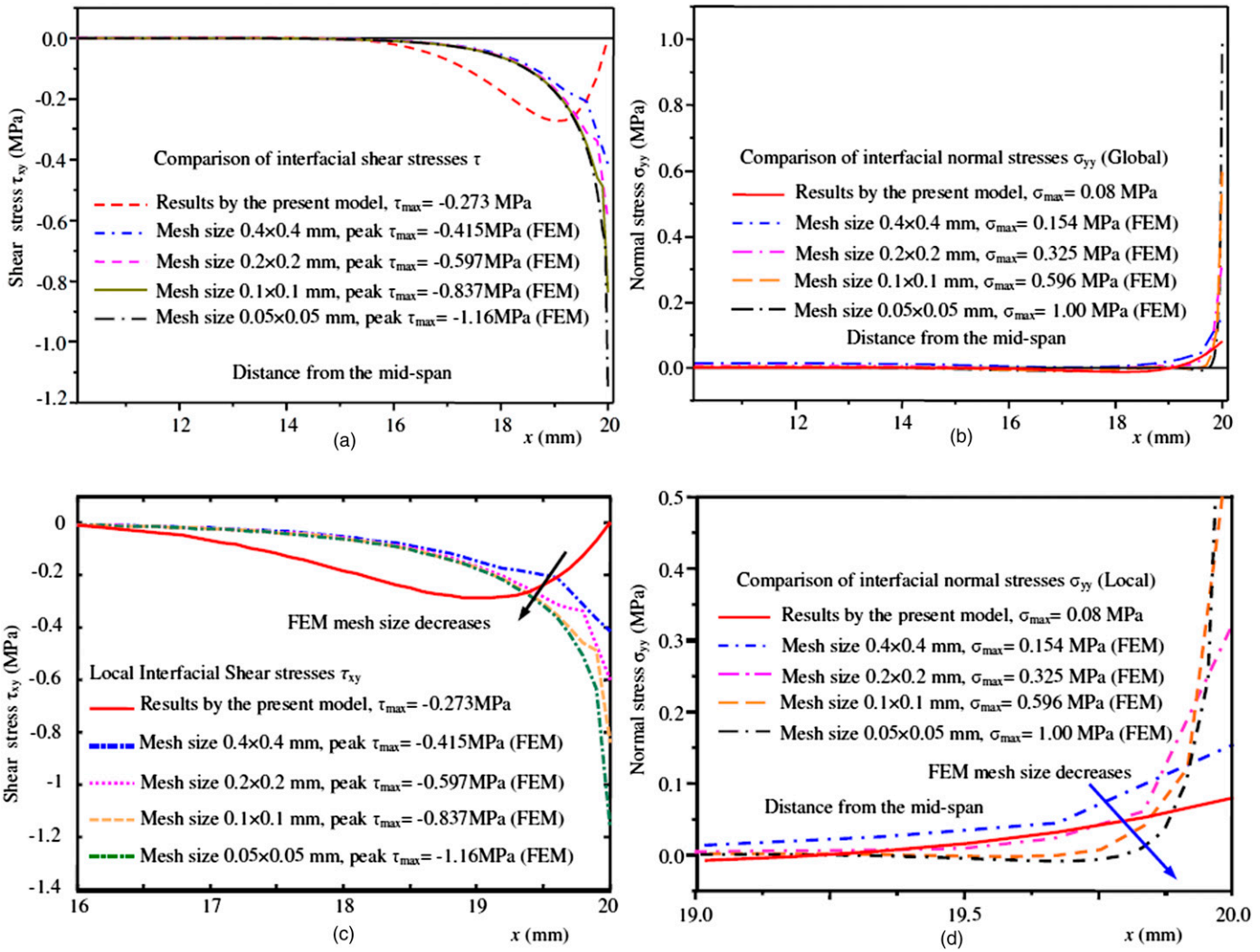


**Fig. 4.** Comparison of interfacial shear and normal stresses predicted by the present method with those by FEM (*ANSYS*): (a) interfacial shear stress $\tau$; (b) interfacial normal stress $\sigma$ (axial tensile stress of the substrate layer: $p_0 = 1$ MPa); (c) zoomed interfacial shear stress $\tau$ of case (b) near adherend end; (d) zoomed interfacial normal stress $\sigma$ of case (b) near adherend end

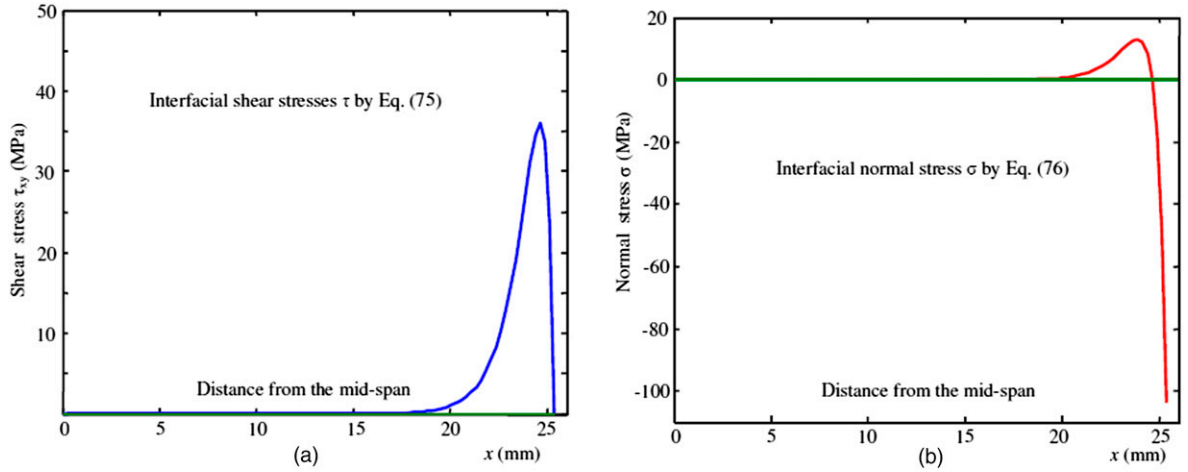


**Fig. 5.** Interfacial shear and normal stresses of bimaterial thermostat subjected to uniform change of temperature: (a) shear stress $\tau$; (b) normal stress $\sigma$



J. Eng. Mech.

the two interfacial stress functions $f(x)$ and $g(x)$ as independent functions by eliminating the assumption in Eq. (7). As a result, the accuracy of interfacial stresses improved although the process was much more complex and no explicit expressions of these interfacial stresses were available. In the case of the same bonded joint subjected to the same change of temperature, the high-order solution by Wu and Jenson (2011) gave the peak interfacial shear and normal stresses as $\tau_{\max} = 69.32$ MPa and $\sigma_{\max} = 117.70$ MPa, respectively. It can be observed that the peak interfacial normal stress is accurately predicted by the present low-order method whereas the interfacial shear stress is underestimated. Furthermore, the present method predicts that the profiles of interfacial shear and normal stress distributions are very similar to those predicted by the high-order method (Wu and Jenson 2011). Thus, in the view of scaling analysis, the present semianalytic solution to the interfacial stresses in bonded joints have advantages due to their simplicity and explicit expressions of the stress components.

Based on the formulas developed earlier, a wide stress spectrum of bonded joints with varying material composition as well as length and thickness ratios can be determined conveniently in closed form following the presented approach. The stress distribution gained from this process could be used for strength analysis and structural optimization of bonded joints. The stress expressions obtained in this study can be used for efficient scaling analysis such as examination of the effect of a specific material and geometrical parameter of adherends on the stress distribution. Moreover, the formalism proposed in this study can be conveniently generalized for stress analysis of broad bonded joints involving more general loading cases such as the typical single/double adhesively bonded lap and strap joints as well as multilayered composite joints subjected to combined mechanical and thermal loads.

## Concluding Remarks

A new semianalytic stress-function variational approach has been formulated to the interfacial stresses of bonded joints subjected to axial tension and uniform change of temperature. In the process, all the stress components were approximated in terms of two unknown interfacial shear and normal stress functions $f$ and $g$ based on the classic beam theory and 2D elasticity. The interfacial stress functions $f$ and $g$ were correlated through the deformation compatibility of the joint. Minimization of the complementary strain energy of the joint resulted in a fourth-order ODE of the interfacial shear stress $f$. Advantages of the current interfacial stress solutions include that all the stresses are determined in explicit expressions, all the BCs are satisfied, and all the material and dimensional parameters have been incorporated into the solutions. Thus, the present model gives a refined understanding of the scaling behavior of stress variation in bonded joints. The current stress solutions can recover those given by the elementary beam theory in the limiting case. Validity of the present model made by FEA and comparison with results reported in the literature guarantees the application of the present model for scaling analysis of stresses in bonded joints subjected to mechanical and thermomechanical loads.

The analytic approach developed in this work can be conveniently generalized for a variety of bonded structures and materials where the interfacial edge stresses dictate the strength and durability of the structures and components of interest.

## Acknowledgments

Partial support of this work by a National Aeronautics and Space Administration (NASA) Experimental Program to Stimulate Competitive Research (EPSCoR) seed grant and the North Dakota State University Centennial Development Foundation (2010) is gratefully appreciated.

## References

*ANSYS 12.0.1* [Computer software]. Canonsburg, PA, Ansys.

Beer, F., Johnston, E. R., Dewolf, J. T., and Mazurek, D. F. (2009). *Mechanics of materials*, 5th Ed., McGraw Hill, New York.

Carpinteri, A., Cornetti, P., and Pugno, N. (2009). "Edge debonding in FRP strengthened beams: Stress versus energy failure criteria." *Eng. Struct.*, 31(10), 2436–2447.

Chang, F. V. (1990). "Interlaminar stresses of laminated composite joints with double cover plates." *Int. J. Solids Struct.*, 26(4), 437–453.

Chang, F. V. (1993). *Interlaminar stresses on composite materials*, High Education Press, Beijing.

Chen, D., and Cheng, S. (1992). "Torsional stress in tubular lap joints." *Int. J. Solids Struct.*, 29(7), 845–853.

Chen, W. T., and Nelson, C. W. (1979). "Thermal stress in bonded joints." *IBM J. Res. Develop.*, 23(2), 179–188.

da Silva, L. F. M., das Neves, P. J. C., Adams, R. D., and Spelt, J. K. (2009a). "Analytic models of adhesively bonded joints—Part I: Literature survey." *Int. J. Adhes. Adhes.*, 29(3), 319–330.

da Silva, L. F. M., das Neves, P. J. C., Adams, R. D., Wang, A., and Spelt, J. K. (2009b). "Analytic models of adhesively bonded joints—Part II: Comparative study." *Int. J. Adhes. Adhes.*, 29(3), 331–341.

De Lorenzis, L., and Teng, J. G. (2007). "Near-surface mounted FRP reinforcement: An emerging technique for strengthening structures." *Composites Part B*, 38(2), 119–143.

Eischen, J. W., Chung, C., and Kim, J. H. (1990). "Realistic modeling of edge effect stresses in bimaterial elements." *J. Electron. Packag.*, 112(1), 16–23.

Gates, B. D. (2009). "Flexible electronics." *Science*, 323(5921), 1566–1567.

Goland, M., and Reissner, E. (1944). "The stresses in cemented joints." *J. Appl. Mech.*, 11(1), 17–24.

Hutchinson, J. W., and Suo, Z. (1992). "Mixed mode cracking in layered materials." *Adv. Appl. Mech.*, 29(1), 63–194.

Jiang, H. Q., et al. (2008). "Finite width effect of thin-films buckling on compliant substrate: Experimental and theoretical studies." *J. Mech. Phys. Solids*, 56(8), 2585–2598.

Jiang, H. Q., Khang, D. Y., Song, J. Z., Sun, Y. G., Huang, Y. G., and Rogers, J. A. (2007). "Finite deformation mechanics in buckled thin films on compliant supports." *Proc. Natl. Acad. Sci.*, 104(40), 15607–15612.

Jones, M. R. (1999). *Mechanics of composite materials*, 2nd Ed., Taylor & Francis, Philadelphia.

Khang, D. Y., Jiang, H. Q., Huang, Y., and Rogers, J. A. (2006). "A stretchable form of single-crystal silicon for high-performance electronics on rubber substrates." *Science*, 311(5758), 208–212.

Khang, D. Y., Rogers, J. A., and Lee, H. H. (2009). "Mechanical buckling: Mechanics, metrology, and stretchable electronics." *Adv. Funct. Mater.*, 19(10), 1526–1536.

Kim, D. H., and Rogers, J. A. (2008). "Stretchable electronics: Materials strategies and devices." *Adv. Mater.*, 20(16), A1–A16.

Li, X. F. (2001). "Closed-form solution for a mode-III interface crack between two bonded dissimilar elastic layers." *Int. J. Fract.*, 109(2), 3–8.

Lu, N. S., Yoon, J., and Suo, Z. G. (2007). "Delamination of stiff islands patterned on stretchable substrates." *Int. J. Mater. Res.*, 98(8), 717–722.

Ru, C. Q. (2002). "Interfacial thermal stresses in bimaterial elastic beams: Modified beam models revisited." *J. Electron. Packag.*, 124(3), 141–146.

Sih, G. C. (1973). *Handbook of stress intensity factors*, Lehigh Univ., Bethlehem, PA.

Song, J., et al. (2008). "Buckling of a stiff thin film on a compliant substrate in large deformation." *Int. J. Solids Struct.*, 45(10), 3107–3121.

Suhir, E. (1986). "Stresses in bi-metal thermostats." *J. Appl. Mech.*, 53(3), 657–660.
Suhir, E. (1989). "Interfacial stresses in bimaterial thermostats." *J. Appl. Mech.*, 56(3), 595–600.
Sun, Y. G., Choi, W. M., Jiang, H. Q., Huang, Y. G., and Rogers, J. A. (2006). "Controlled buckling of semiconductor nanoribbons for stretchable electronics." *Nat. Nanotechnol.*, 1(2), 201–207.
Suo, Z. G., and Hutchinson, J. W. (1990). "Interface crack between two elastic layers." *Int. J. Fract.*, 43(1), 1–18.
Tada, H., Paris, P. C., and Irwin, C. G. (1973). *The stress analysis of cracks*, Del Research, Hellertown, PA.
Timoshenko, S. (1925). "Analysis of bi-metal thermostats." *J. Opt. Soc. Am.*, 11(3), 233–255.
Timoshenko, S., and Goodier, J. N. (1951). *Theory of elasticity*, 2nd Ed., McGraw Hill, New York.
Wu, X. F. (2009). *Fracture of advanced composites with nanostructured interfaces: Fabrication, characterization and modeling*, VDM, Germany.
Wu, X. F., and Dzenis, Y. A. (2002a). "Closed-form solution for a mode-III interfacial edge crack between two bonded dissimilar elastic strips." *Mech. Res. Commun.*, 29(5), 407–412.
Wu, X. F., and Dzenis, Y. A. (2002b). "Closed-form solution for the size of plastic zone in an edge-cracked strip." *Int. J. Eng. Sci.*, 40(15), 1751–1759.
Wu, X. F., and Dzenis, Y. A. (2005). "Experimental determination of probabilistic edge-delamination strength of a graphite-fiber/epoxy composite." *Compos. Struct.*, 70(1), 100–108.
Wu, X. F., Dzenis, Y. A., and Fan, T. Y. (2003a). "Two semi-infinite interfacial cracks between two bonded dissimilar elastic strips." *Int. J. Eng. Sci.*, 41(15), 1699–1710.
Wu, X. F., Dzenis, Y. A., and Gokdag, E. (2004). "Edge-cracked orthotropic bimaterial butt joint under anti-plane singularity." *Int. J. Nonlinear Sci. Numer. Simul.*, 5(4), 347–354.
Wu, X. F., Dzenis, Y. A., and Strabala, K. W. (2008). "Free-edge stresses and progressive cracking in surface coatings of circular torsion bars." *Int. J. Solids Struct.*, 45(7–8), 2251–2264.
Wu, X. F., Dzenis, Y. A., and Zou, W. S. (2003b). "Interfacial edge crack between two bonded dissimilar orthotropic strips under antiplane point loading." *Z. Angew. Math. Mech.*, 83(6), 419–422.
Wu, X. F., and Jenson, R. A. (2011). "Stress-function variational method for stress analysis of bonded joints under mechanical and thermal loads." *Int. J. Eng. Sci.*, 49(3), 279–294.
Wu, X. F., Jenson, R. A., and Zhao, Y. H. (2014). "Stress-function variational approach to the interfacial stresses and progressive cracking in surface coatings." *Mech. Mater.*, 69(1), 195–203.
Wu, X. F., and Zhao, Y. H. (2013). "Stress-function variational method for interfacial stress analysis of adhesively bonded joints." *Int. J. Solids Struct.*, 50(25–26), 4305–4319.
Yang, C., and Guan, Z. D. (2009). "Stress analysis of composite pipe joints under combined tensional and tensile loading." *J. Pressure Vessel Technol.*, 131(5), 051210.
Yang, C., Huang, H., Tomblin, J. S., and Sun, W. J. (2004). "Elastic-plastic model of adhesive-bonded single-lap composite joints." *J. Compos. Mater.*, 38(4), 293–309.
Yin, W. L. (1994a). "Free edge effects in anisotropic laminates under extension, bending and twisting. Part I: A stress-function-based variational approach." *J. Appl. Mech.*, 61(2), 410–415.
Yin, W. L. (1994b). "Free edge effects in anisotropic laminates under extension, bending and twisting. Part II: Eigenfunction analysis and the results for symmetric laminates." *J. Appl. Mech.*, 61(2), 416–421.
Yoon, J., Zhang, Z., Lu, N. S., and Suo, Z. G. (2007). "The effect of coating in increasing the critical size of islands on a compliant substrate." *Appl. Phys. Lett.*, 90, 211912.
Yu, H. H., and Hutchinson, J. W. (2001). "Edge effects in thin film delamination." *Acta Mater.*, 49(1), 93–107.
Yu, H. H., and Hutchinson, J. W. (2003). "Delamination of thin film strips." *Thin Solid Films*, 423(1), 54–63.
Yuan, H., Teng, J. G., Seracino, R., Wu, Z. S., and Yao, J. (2004). "Full-range behavior of FRP-to-concrete bonded joints." *Eng. Struct.*, 26(5), 553–565.